Image-Based Robotic System for Enhanced Minimally Invasive Intra-Articular Fracture Surgeries

G. Dagnino, I. Georgilas, P. Köhler, R. Atkins, and S. Dogramadzi

***Abstract*— Robotic assistance can bring significant improvements to orthopedic fracture surgery: facilitate more accurate fracture fragment repositioning without open access and obviate problems related to the current minimally invasive fracture surgery techniques by providing a better clinical outcome, reduced recovery time, and health-related costs. This paper presents a new design of the robot-assisted fracture surgery (RAFS) system developed at Bristol Robotics Laboratory, featuring a new robotic architecture, and real-time 3D imaging of the fractured anatomy. The technology presented in this paper focuses on distal femur fractures, but can be adapted to the larger domain of fracture surgeries, improving the state-of-the-art in robot assistance in orthopedics. To demonstrate the enhanced performance of the RAFS system, 10 reductions of a distal femur fracture are performed using the system on a bone model. The experimental results clearly demonstrate the accuracy, effectiveness, and safety of the new RAFS system. The system allows the surgeon to precisely reduce the fractures with a reduction accuracy of 1.15 mm and 1.3°, meeting the clinical requirements for this procedure.**

I. Introduction

Surgical procedures require a high degree of capability, efficiency, and safety for both the patient and the surgeon [1]. The treatment of lower limb joint fractures consists in anatomical surgical reduction involving an open incision (Fig.1a) into the joint. The anatomical reduction of a fracture is achieved by positioning and aligning the fragments of the broken bone to reconstruct the fractured bone as precisely as possible, so that the bone recovers to a form as close as possible to its original form ensuring the correct functionality again. After the reduction, the fragments are rigidly fixed together using a metallic plate and screws, or intramedullary nails [2]. Although this open procedure can be effective, it is associated with extensive damage to the soft tissues, slow bone healing and increased risk of infection, with consequent prolonged hospitalization, rehabilitation time, and health-related costs [3]. Minimally invasive surgical techniques (i.e. percutaneous) have been developed to mitigate the problems related with open surgery. These techniques involve fragment manipulation using pins inserted in the fragments through small incisions in the patient's flesh (Fig.1b). Such techniques are associated with a faster recovery and a lower risk of infection compared to open surgery techniques [4].

G. Dagnino*, I. Georgilas, P. Köhler, and S. Dogramadzi are with the Bristol Robotics Laboratory, Coldharbour Lane, Frenchay, BS16 1QY, Bristol, United Kingdom (*corresponding author, phone: +44-0117-32-86375; email: giulio.dagnino@uwe.ac.uk). R. Atkins is with the University Hospitals Bristol, UK (email: Roger.Atkins@sneydwood.co.uk).

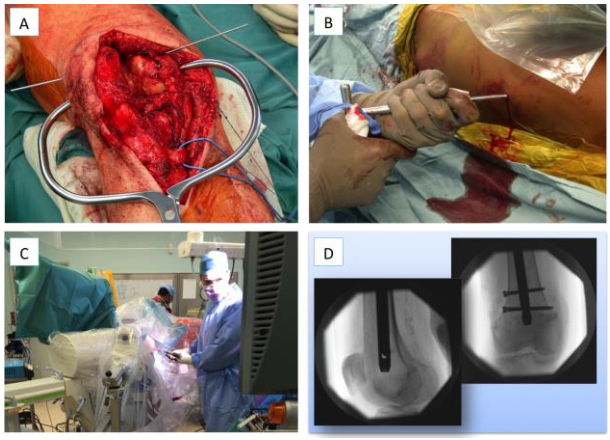

Fig.1 Example of distal femur fracture surgical procedures: open surgery (A); minimally invasive surgery (B); current setup for minimally invasive fracture surgery (C); and two examples of intra-operative fluoroscopic images (D).

However, the major challenge in minimally invasive fracture surgery (MIFS) using the current surgical setup (Fig.1c) is to deduce the desired reduction position of bone fragments from multiple intraoperative fluoroscopic images of the fracture. The 2D nature of these images (Fig.1d), the localized and limited 2D-field of view, and their low resolution, do not provide enough information to the surgeon with respect to the fracture alignment and rotation, which is essentially a three-dimensional problem. Also, the high forces occurring during the reduction process increase the physical load on the surgeon preventing the reduction movements [5] and occasionally resulting in suboptimal fracture reduction [3].

Robotic assistance can actually have a positive impact in overcoming the issues identified above. Manipulating joint-related bone fragments to a high positional accuracy is a complex problem. Several research solutions have been proposed for long bone fracture reduction (specifically femur shaft fractures). Warisawa *et al.* [6] proposed a fracture reduction robot whose design concept seems to be difficult or impossible to utilize it for other fracture types. Westphal *et al.* [7] reported on a robotic system for the reduction of femur shaft fractures based on a telemanipulated industrial serial robot prone to positional errors due to closing the control loop through the surgeon. Tang *et al.* [8] and Wang *et al.* [9], utilized a parallel-robot for the reduction of diaphyseal femur fractures. All the described systems are restricted to long bone fractures, attempting to solve a different problem from intra articular fractures that involve joints and typically require higher reduction accuracy [10]. Long bone fractures

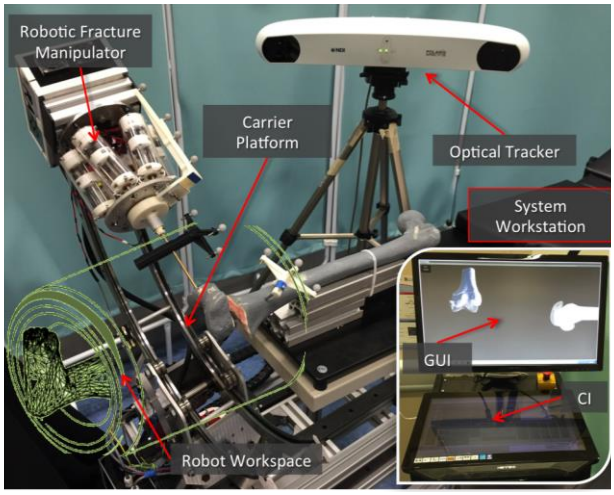

Fig.2 The new RAFS system concept.

have smaller number of larger fragments that present a 2D problem for surgical reduction and are perceived to be easier to manage in the clinical setting. Intra-articular fractures are 3D fractures and are, therefore, more difficult to solve using 2D intra-operational images.

Robot-assisted fracture surgery (RAFS) is the focus of new research at Bristol Robotics Laboratory (BRL). Raabe *et al.* [11] developed the first robotic prototype for semi-automatic percutaneous reduction of intra-articular knee fractures using parallel-robots for fragment manipulation. The robots are controlled using proprioceptive position feedback and have only been tested on bone phantoms (Sawbones). The key limitations of the system include the lack of closed-loop position control, no force-feedback, limited operational workspace, the lack of real-time intra-operative 3D imaging, and the need of intra-operative CT scan. This restricted the system's reliability and usability in a real surgical environment. This paper presents a redesign (Fig.2) of the first RAFS system prototype, which is improved by introducing new robotic architecture with increased operational workspace, new control system strategy enabling closed-loop control and force feedback, and new real-time 3D imaging which removes the need of intra-operative CT scan from the clinical workflow.

II. Clinical Requirements

Clinical requirements were established through discussions with orthopedic surgeons and analysis of various fracture cases [10]. Distal femur fractures with fragment dislocations bigger than 5° rotational and 1mm translational displacements should be treated surgically. High impact fractures can cause dislocations of more than 2 cm and 60-180°. During surgical reduction the fracture fragments are typically approached through the anterior (front) of the limb $\pm 120^{o}$ from its vertical axis or from the lateral or medial side $\pm 60^{o}$ around the side axes of the limb. Based on this geometrical requirement, an optimal robot workspace should have a hollow hemispheric shape (green sketch in Fig.2). The required load capacity for the system has been defined by in vivo measured forces applied by surgeons during lower limb surgical procedures. We instrumented a periosteal elevator and a traction table with two 6-DOF load cells, developed a dedicated data acquisition software, and analyzed the force/torque data as reported in [12]. The procedures consisted of manipulating bone fragments using the instrumented device and collecting relative force/torque data. A summary of the clinical requirement is reported in Table 1.

TABLE I. Clinical Requirements

Parameter	Value
Reduction Accuracy (Translational)	< 1mm
Reduction Accuracy (Rotational)	< 5°
Translational Workspace x, y, z	±25mm
Rotational Workspace $\vartheta_x, \vartheta_y, \vartheta_z$	±90°, ±60°, ±30°
Forces/Torques for Manipulating Fragments	~ 20N (force) ~ 2Nm (torque)

III. Surgical System Concept

Through discussion and interaction with orthopedic surgeons, we defined three aspects to be key in surgeons' expectation for RAFS: (1) Improved reduction accuracy: required to precisely align the broken fragment and restore the joint functionality; (2) Minimized soft tissue damage: required for a better clinical outcome in terms of articular stiffness and post-traumatic arthritis; and (3) Enhanced intra-operative visualization: required to better understand the three-dimensional fracture configuration in real-time. The new RAFS system is designed to address the above aspects. The main elements of the system (Fig.2) are:

Robotic Fracture Manipulator (RFM): this device, introduced in [13], is designed to be connected to the bone fragment through an orthopedic pin for fragment manipulation. This component, based on parallel-robot configuration with 6-DOF, has 6 motorized linear actuators fully computer-controlled and is able to realize accurate positioning within its workspace *(±10.25mm* along x, y, *±15mm* along z and rotational limits of *±17°* around each axis). It provides a *0.03±0.01mm* translational accuracy and a *0.12±0.01°* rotational accuracy [14]. The device mounts a 6-DOF force-torque load cell enabling force control. In order to fully cover the required operational workspace (Table1, Fig.2), the robotic manipulator is mounted on a carrier platform.

Carrier Platform (CP): this device is used for the coarse positioning of the RFM (which is connected to it) close to the orthopedic pin (accuracy ~5mm, ~5°), allowing the surgeon's assistant to connect the RFM to the pin. The RFM is then used to accurately manipulate the fragment to the desired, i.e. reduced, pose. The CP has 4-DOF, two prismatic and two revolute (see Fig.4a), and a cylindrical workspace (700mm length, 300mm diameter), covering the required operational workspace described in Section II and shown Fig.2. The CP has 4 motorized actuators, one for each DOF, and it is fully computer-controlled.

System Workstation: it employs a host-target structure composed by a PC (host) and a real-time controller with FPGA (target), and a low-level motor controller. The host PC runs the Graphical User Interface (GUI) and the

Configuration Interface (CI). It creates the link between the surgical team and the robotic system. The GUI allows the surgeon to interact with the 3D Imaging System, while the CI is used for system configuration and safety alarm messages. We adopted two separate screens: the GUI is displayed on a large 3D monitor dedicated to the surgeon, while the CI is displayed on a touchscreen interface to allow a surgical assistant to change the settings configuration without requiring the surgeon's intervention. The host PC communicates with the target controller via ethernet. The target controller (NI-compactRIO 9068, National Instruments) process users' commands and sends the motion commands to the low level motor controller (EPOS 2 24/3, Maxon Motor) that executes the movement of the robotic system.

3D Imaging System: this system, introduced in [15] consists of a reduction software, an optical tracking system, and a user controller. The reduction software receives pre-operative CT scan data of the fracture and generates the 3D models of the bone fragments. The GUI displays the 3D models and allows the surgeon to interact with them by using a controller for intra-operative planning of fracture reduction, i.e. virtual reduction. Collision avoidance is enabled to avoid overlap of the 3D models. The optical tracking system (Polaris Spectra, NDI Inc.) provides in real-time (25Hz) the pose of optical tools (*0.25mm* accuracy) connected to the bone fragments and the RFM, i.e. using optical markers placed according to a known geometry (refer to Section V).

This configuration provides the following benefits: (1) the robotic fracture manipulator improves fracture reduction accuracy; (2) the percutaneous access to the fracture through orthopedic pins guarantees the minimum damage to soft tissue; and (3) the pre-planned virtual reduction of the fracture and the force feedback provided by the load cell further improve the precision and safety.

IV. Control Architecture

The overall architecture of the RAFS system is based on a host-target configuration [14]. The surgical team is always in control of the entire system through the GUI and the CI. The surgeon plans the surgical procedure from the system workstation by virtually reducing the fracture. The high-level controller processes the surgeon's commands and generates the motion commands for the robot to achieve the planned reduction. These commands are sent to the low-level controller that executes the movement of the robotic manipulator, realizing the physical reduction of the fracture. The robot controller has been designed and implemented as shown in Fig.3. Position control of the proposed surgical system is based on a combination of open-loop and closed-loop position controllers [16]. An open-loop control uses individual motor encoders to control the robot's pose (RFM and CP) in the task space. External position measurements are necessary for the overall system accuracy and repeatability: visual feedback is gained by optical tracking data in order to implement closed-loop vision-based control on the RFM by placing an optical tool on its end-effector.

Force/Torque feedback is gained by the 6DOF load cell mounted on the end-effector of the RFM. These feedback data are used as a safety feature for the system (Fig.3): if the measured force-torque data $\boldsymbol{F}_a$ exceed predefined [12] safety thresholds $\boldsymbol{F}_{th}$, then the force controller immediately stops the movement of the robot to avoid damages to the patient.

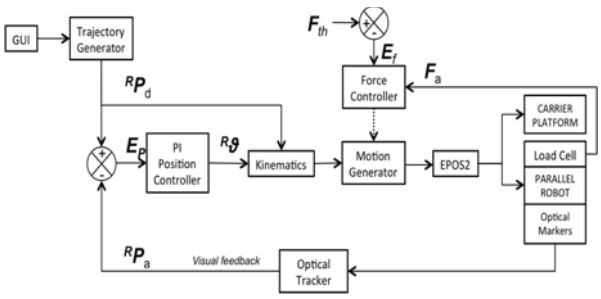

Fig.3 Control circuit block diagram.

A. Kinematics and Open Loop Control

The open-loop control of the robotic system is based on the kinematics of the CP and the RFM (Fig.4). The surgeon defines the desired (*d*) pose for the RFM $^{RFM}\boldsymbol{P_d}$ through the GUI by virtually reducing the fracture as described in Section V. The initial and the desired positions of the RFM are now defined by solving the kinematics, first for the CP for the positioning of the RFM within the operational workspace, and then for the RFM for the fine positioning of the bone fragment. The task space *trajectory generator* generates a desired trajectory for the CP and RFM, while the *kinematics* calculates the motion commands for their motors to reach the desired pose $^{RFM}\boldsymbol{P_d}$. The forward kinematics of the CP is based on the Denavit–Hartenberg (DH) analysis (Fig.4a). The DH parameters are given based on the joint vector:

$$\boldsymbol{q} = [L_z \; L_y \; T \; R] \tag{1}$$

where, L_z is the linear motion along the axis of the limb, L_y is the linear motion perpendicular to L_z, T is the tilting revolute joint around L_y, and R is the revolute rotation around L_z, as shown in Fig.4a.

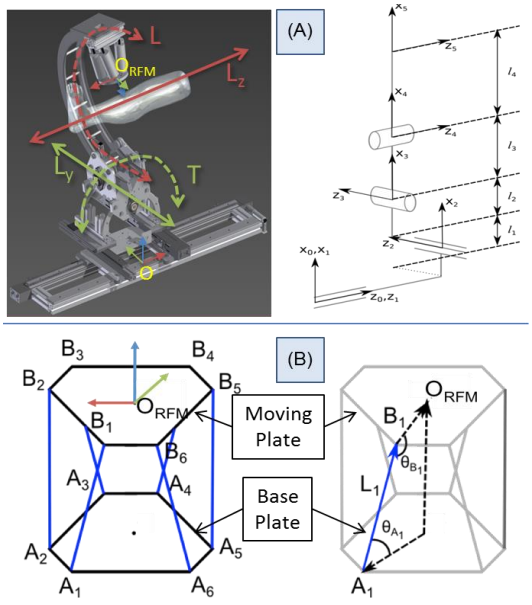

Fig.4 Kinematics for the proposed system: the carrier platform (A), and the robotic fracture manipulator (B).

The transformation matrix between the CP origin (O) and the RFM origin (O_{RFM}) is given by:

$$
{}^{O}\boldsymbol{T}_{O_{RFM}} = \begin{bmatrix} {}^{O}R_{O_{RFM}} & {}^{O}P_{O_{RFM}} \\ 0 \quad 0 \quad 0 & 1 \end{bmatrix} = \\
= \begin{bmatrix} -s_T & -c_T s_R & -c_R c_T & X_{FK} \\ 0 & c_R & -s_R & Y_{FK} \\ c_T & -s_R s_T & -c_R s_T & Z_{FK} \\ 0 & 0 & 0 & 1 \end{bmatrix} \tag{2}
$$

$$
X_{FK} = l_1 + l_2 + l_3 c_T + l_4 c_R c_T + T_A c_R c_R - T_B c_T s_R
$$

$$
Y_{FK} = T_B c_R - L_y + l_4 s_R + T_A s_R
$$

$$
Z_{FK} = L_Z + l_3 s_T + l_4 c_R s_T + T_A c_R s_T - T_B s_R s_T
$$

where, c_x is *cos(x)*, s_x is *sin(x)*, T_A and T_B are the offsets along x and z axes (given by structural dimensions).

For a desired target position of the connected RFM:

$$
{}^{RFM}\boldsymbol{P}_d = (x_d, y_d, z_d, \theta x_d, \theta y_d, \theta z_d) \tag{3}
$$

analytical solution for the inverse kinematics can be derived by solving the forward kinematics (2) to find CP parameters (refer to (1) and Fig.4a):

$$
\begin{aligned}
R &= \theta z_d \\
T &= \text{acos}\ \frac{x_d - l_1 - l_2 - T_A c_R c_T}{(l_3 + l_4 c_R - T_B s_R)} \\
L_y &= T_B c_R + l_4 s_R + T_A s_R - y_d \\
L_Z &= Z_{FK} - l_3 s_T - l_4 c_R s_T - T_A c_R s_T + T_B s_R s_T
\end{aligned} \tag{4}
$$

The RFM has a parallel-robot configuration with six struts. The inverse kinematics is derived using a loop closure approach for each strut (Fig.4b). Given a desired position input the correspondent length of the i^{th} strut can be calculated as described in [13]. The generated motion data for the CP and the RFM are sent to low-level controllers (CAN data through the FPGA) which control the motorized actuators to reach the desired pose.

B. Closed-Loop Control

Once the RFM is positioned and the desired pose ${}^{RFM}\boldsymbol{P}_d$ is reached using the open-loop control, the actual pose of the RFM ${}^{RFM}\boldsymbol{P}_a$ provided by the optical tracker is compared to the desired pose ${}^{RFM}\boldsymbol{P}_d$ which generates the pose error $\boldsymbol{E_P} = (\boldsymbol{E_T}, \boldsymbol{E_R})$. The translational error $\boldsymbol{E_T}$ is simply the difference between the desired and the actual for each axis:

$$
\boldsymbol{E_T} = \begin{bmatrix} x_d - x_a \\ y_d - y_a \\ z_d - z_a \end{bmatrix} \tag{5}
$$

For orientation control $\boldsymbol{E_R}$, the quaternion error $\boldsymbol{Q_e}$ is computed using the quaternion product between the desired quaternion ${}^{RFM}\boldsymbol{Q}_d$ and the inverse of the actual quaternion ${}^{RFM}\boldsymbol{Q}_a$ provided by the optical tracker for each axis [17].

$$
\boldsymbol{Q_e} = ({}^{RFM}\boldsymbol{Q_a})^{-1} \times {}^{RFM}\boldsymbol{Q_d} = \begin{bmatrix} w_x & a_x & 0 & 0 \\ w_y & 0 & b_y & 0 \\ w_z & 0 & 0 & c_z \end{bmatrix} \tag{6}
$$

$$
\boldsymbol{E_R} = \begin{bmatrix} \text{acos}(w_x) \\ \text{acos}(w_y) \\ \text{acos}(w_z) \end{bmatrix}
$$

where, w_i,a_x,b_y,c_z are components of the quaternions [17].

When the elements of $\boldsymbol{E_T}$ are less or equal to 0.25 mm and the elements of $\boldsymbol{E_R}$ are less or equal to 0.25°, the robot's pose is considered acceptable and the target is reached. Otherwise the vision-based system is activated to correct the pose as shown in Fig.3. This system is composed of six proportional and integral (PI) controllers, one for each translation (x, y, z) and rotation (θx, θy, θz) axis of the end-effector in the task frame. It is based on a PI control law [18] and generates motion commands ${}^{RFM}\boldsymbol{\phi} = (\phi_x, \phi_y, \phi_z, \phi_{\theta x}, \phi_{\theta y}, \phi_{\theta z})$ to adjust the pose of the end-effector. These motion commands generated by the PI controllers are sent to the *kinematics* block, then to the *motion generator* (as described in the *"Kinematics and Open Loop Control"* sub-section) at each processing time step n using (7):

$$
\phi(n) = k_p \cdot E(n) + k_I \cdot E_I(n) \tag{7}
$$

where:

$$
E_I(n) = E_I(n-1) + \frac{E(n)+E(n-1)}{2}\Delta t \tag{8}
$$

where $E_I(n)$ is the integral error, k_P is the proportional control gain, k_I is the integral gain, and Δt is the sampling time. In the proposed system the following constants were selected after tuning [19]: $k_P = 50$; $k_I = 18$; $\Delta t = 20$ms. When the closed-loop control is used, the *motion generator* system creates new actual velocity profiles for each linear actuator at each processing time n based on the new actual position of the robot end-effector provided by the optical tracker; closer to the desired pose the robot gets, the smaller is the actual velocity of each actuator. This means that the actuators' actual velocity profiles decrease as the robot reaches its desired pose.

V. Clinical Workflow

Figure 5 shows the clinical workflow for the reduction of a joint fracture using the RAFS system. Complete two-part distal femur fractures (Salter-Harris type I fracture [20]) (Fig.6a) have been used for the development, experimental validation, and proof of concept of the proposed surgical system. The procedure starts with the insertion of the orthopedic pins P1 and P2 into each bone fragment by the surgeon. These pins will allow fragment manipulation. Then, pre-operative CT scan of the fracture and inserted pins is taken, and the resulting dataset segmented to generate 3D models (STL format) of each bone fragment and the inserted pins. These models are imported in the reduction software (Fig.6b), concluding the pre-operative part of the workflow. In the operating theatre (Fig.6c), one optical tool (T1) is placed on the orthopedic pin (P1) inserted in fragment 1 (F1), and a second optical tool (T2) is placed on the orthopedic pin (P2) inserted in the reference bone (F2). A further optical tool

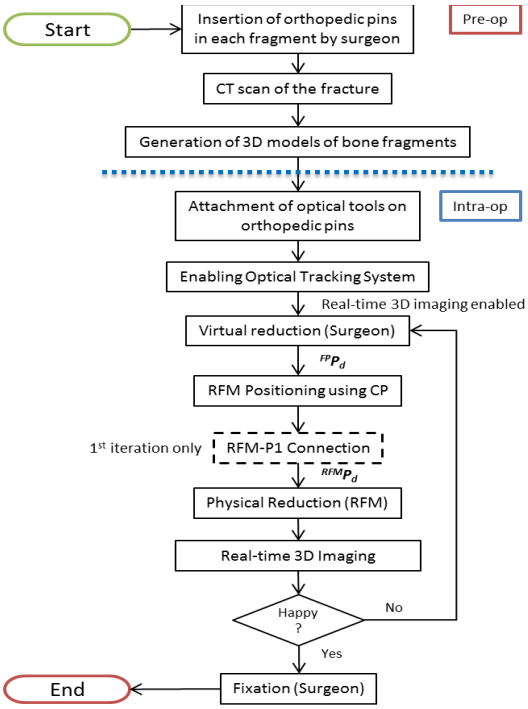

Fig.5 Clinical workflow for the RAFS system.

(TR) is placed on the RFM. The orthopedic pins P1 and P2 were designed to be connected in a unique way to the optical tools T1 and T2 (Fig.6c), having their coordinate frames coincident, i.e. $CF_{Pi} \equiv CF_{Ti}$. Therefore, the optical tracker provides the actual poses of F1 (by tracking P1), F2 (by tracking P2), and RFM (by tracking TR), enabling the intra-operative real-time imaging as described in [15]. The surgeon virtually reduces the fracture using the reduction software GUI (Fig,7b) by matching F1 and F2 (intra-operative planning). This process generates the desired pose ${}^{FP}\boldsymbol{P_d}$ for F1-P1. Then, the system moves the CP in order to position the RFM close to the orthopedic pin P1 between its current location (provided by T1) and the final anatomically correct position ${}^{FP}\boldsymbol{P_d}$. A surgeon's assistant rigidly connects P1 to the RFM, and the reduction software - based on the relative position of P1 (by tracking T1) with respect to the RFM (by tracking TR) - calculates the desired pose ${}^{RFM}\boldsymbol{P_d}$ for the RFM in the task space, based on the desired pose ${}^{FP}\boldsymbol{P_d}$ for F1 in the image space, as reported in [15]. Finally, the RFM executes the desired movement for F1 to achieve the physical reduction of the fracture, while reference bone F2 remains fixed. The real-time imaging updates the actual pose of the fragments, and the surgeon checks intra-operatively the reduction in 3D without the use of any other imaging device. If the reduction is acceptable, the surgeon proceeds with the fixation of the fracture, and the surgery ends.

VI. Experimental Validation

To demonstrate the enhanced performance of the RAFS system, 10 reductions of a distal femur fracture were performed following the clinical workflow described in Section V and the experimental setup shown in Fig.6. Two orthopedic pins (P1 and P2) were inserted in an unbroken femur model (Sawbones). Before proceeding with the CT imaging, the relative pose of F1 with respect to F2 in the unbroken configuration was obtained using the optical

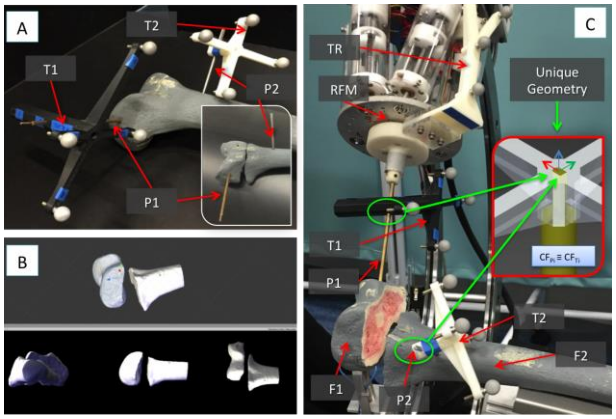

Fig.6 Experimental setup. Fractured femur model with orthopedic pins inserted (A); reduction software GUI (B); the RFM is connected to the bone fragments through the orthopedic pins; optical tool are attached in a unique way to the pins allowing for real-time imaging (C).

tracker, T1 and T2, and represented the target point for the robot in order to reduce the fracture, i.e. the ground truth ${}^{F}\boldsymbol{P_{goal}}$ to check the reduction. Subsequently, the femur was fractured in two fragments (F1 and F2), with P1 inserted in F1 and P2 in F2 (Fig.6a), and CT scanned. 3D models of the fragments and the pins were generated and imported in the reduction software, and the optical tool enabled providing the real-time imaging. A surgeon was asked to virtually reduce the fracture 10 times, by manipulating F1 to match F2. Once the surgeon completed each reduction, the final (i.e. desired) pose ${}^{FP}\boldsymbol{P_d}$ of F1-P1 in the image space was calculated. The CP positioned the RFM close to P1, which was then connected to the RFM, as described in Section V (Fig.6c). The reduction software calculated the desired pose ${}^{RFM}\boldsymbol{P_d}$ for the RFM in the task space. Finally, the robot executed the physical reduction, and the actual pose of F1 (${}^{F}\boldsymbol{P_a}$) and of the RFM (${}^{RFM}\boldsymbol{P_a}$) after the reduction was measured by the optical tracker. This allowed the objective evaluation of the RAFS system measured as: (1) *fragment positioning accuracy:* translational and rotational errors between the desired pose (${}^{FP}\boldsymbol{P_d}$) and the actual pose (${}^{F}\boldsymbol{P_a}$) of F1; (2) *virtual reduction accuracy:* translational and rotational errors between the ground truth pose (${}^{F}\boldsymbol{P_{goal}}$) and the actual pose of F1 after the virtual reduction (${}^{FP}\boldsymbol{P_d}$); (3) *physical reduction accuracy:* translational and rotational errors between the ground truth pose (${}^{F}\boldsymbol{P_{goal}}$) and the actual pose of F1 after the physical reduction (${}^{F}\boldsymbol{P_a}$). The metrics chosen for the system evaluation were the root-mean-squared-error (RMSE), the maximum absolute error (MAE) measured during both virtual and physical reduction. Also, the average load applied during the physical reduction was measured to analyze the contact forces and torques between the manipulated fragment and the femur during the reduction. Experimental results are reported in Table 2.

TABLE II. Experimental Validation: Results

Parameter	RMSE*	MAE	Applied Load*
Fragment Positioning Accuracy	*0.24 ± 0.09 mm* *0.19 ± 0.13 °*	*0.44 mm* *0.32 °*	n.a.
Virtual Reduction Accuracy	*1.09 ± 0.8 mm* *1.02 ± 0.01 °*	*1.21 mm* *1.19 °*	n.a.
Physical Reduction Accuracy	*1.15 ± 0.59 mm* *1.3 ± 0.61 °*	*1.25 mm* *1.6 °*	*2.33 ± 0.13 N* *0.01 ± 0.001 Nm*

* Calculated over 10 reductions.

VII. Discussion

The results from the experimental validation trials demonstrated that the RAFS system is able to meet the demanding reduction accuracy requirements for joint fracture surgeries, i.e. 1mm and 5° (Table 1). High values of RMSE and MAE give an account of how far the manipulated fragment is from the desired, i.e. reduced, position. This implies that, in case of real surgeries, the clinical outcome is not optimal. On these metrics, the RAFS system consistently showed values close to the clinical acceptable ones, i.e. 1mm, 5°. The reduction software allowed the surgeon to virtually reduce the fracture with a maximum residual positioning RMSE of 1.09±0.8mm and 1.02±0.01°, which corresponded to physical reduction accuracy RMSE of only 1.15±0.59mm and 1.3±0.61°, when the robot reduced the fracture. This is due to the submillimetric positioning accuracy of the system, which was measured in 0.24±0.09mm and 0.19±0.13° RMSE. Moreover, the measured MAEs further demonstrated that the RAFS system permits excellent reduction accuracies (both virtual and physical), helping to avoid large deviations from the desired reduction. The experiments also demonstrated that the RAFS system has a higher level of reduction accuracy when compared with other systems reported in literature, such as [7], [8], and [9]. The load measured during the physical reduction resulted in average force of 2.33±0.13N and average torque of 0.01±0.001Nm. These low values further corroborate the findings above, i.e. the accurate physical reduction. Higher values of forces and torques, (without the presence of soft tissues around counteracting the reduction [12], [13]) mean that the reduction is not optimal, i.e. the robot is squashing the manipulated fragment into the femur. Low torque values are an indicator of the goodness of the reduction trajectory, i.e. the manipulated fragment does not creep on the femur, but smoothly reaches the desired position.

VIII. Conclusion

In this paper, a new image-guided robotic system was presented. It was created to redesign a previous prototype [11] with the objective of providing improved accuracy and safety for minimally invasive intra-articular fracture surgeries. This was achieved with the new RAFS system: a redesigned robotic architecture, new control system strategy, and new real-time 3D imaging. The surgeon intra-operatively pre-plans the reduction, by manipulating virtual models of the fracture within the reduction software. The robotic system executes the physical reduction based on the surgeon's preplanning. The experimental evaluation clearly demonstrated the accuracy, effectiveness, and safety of the RAFS system (reduction accuracy of 1.15mm and 1.3°).

In the next steps of development, a second robot (RFM+CP) will be included in the system to allow simultaneous manipulation of two fragments, and the reduction of more common distal femur fractures (see [2]) than Salter-Harris type I. Also, we envision the use of the system with other fractures such as neck of femur, ankle, and upper-limb. Finally, further studies are planned in the optimization of the reduction software through the implementation of a full pre-operative planning, and the evaluation of new user controllers. Human cadaveric trials are planned shortly to assess the system in a more realistic clinical condition, and to obtain accuracy data over the conventional surgical approach.

Acknowledgment

This is a summary of independent research funded by the National Institute for Health Research (NIHR)'s Invention for Innovation (i4i) Programme. The views expressed are those of the author(s) and not necessarily those of the NHS, the NIHR or the Department of Health.

References

[1] M. D. O'Toole, K. Bouazza-Marouf, D. Kerr, M. Gooroochurn, and M. Vloeberghs, "A methodology for design and appraisal of surgical robotic systems," *Robotica*, vol. 28, no. 02, p. 297, Mar. 2010.

[2] "Distal Femur Fracture - Reduction and Fixation," *AO Foundation*.

[3] S. Rammelt, M. Amlang, S. Barthel, J.-M. Gavlik, and H. Zwipp, "Percutaneous Treatment of Less Severe Intraarticular Calcaneal Fractures," *Clin. Orthop.*, vol. 468, no. 4, pp. 983–990, Apr. 2010.

[4] P Gaston, E.M. Will, and J.F. Keating, "Recovery of knee function following fracture of the tibial plateau," *J Bone Joint Surg Br*, vol. 87, no. 9, pp. 1233–6, 2005.

[5] J. Buschbaum, R. Fremd, T. Pohlemann, and A. Kristen, "Computer-assisted fracture reduction: a new approach for repositioning femoral fractures and planning reduction paths," *Int. J. Comput. Assist. Radiol. Surg.*, vol. 10, no. 2, pp. 149–159, May 2014.

[6] S. Warisawa, T. Ishizuka, M. Mitsuishi, and N. Sugano, "Development of a femur fracture reduction robot," in *IEEE ICRA 2004*, New Orleans, LA, USA, 2004.

[7] R. Westphal, Winkelbach S, Wahl F, Gösling T, Oszwald M, Hüfner T, and Krettek C, "Robot-assisted Long Bone Fracture Reduction," *The Int J of Robotics Res*, vol. 28, pp. 1259–1278, 2009.

[8] P. Tang, L. Hu, H. Du, M. Gong , and L. Zhang , "Novel 3D hexapod computer-assisted orthopaedic surgery system for closed diaphyseal fracture reduction," *Int J Med Robot*, vol. 8, no. 1, pp. 17–24, 2012.

[9] J. Wang, W. Han, and H. Lin, "Femoral fracture reduction with a parallel manipulator robot on a traction table," *Int J Med Robotics Comput Assist Surg*, 2013.

[10] J.L. Marsh, *Rockwood And Green's Fractures In Adults*, 8th ed., vol. 2. Wolters Kluwer, 2015.

[11] D. Raabe, S. Dogramadzi, and R. Atkins, "Semi-automatic percutaneous reduction of intra-articular joint fractures - an initial analysis," in *IEEE ICRA 2012*, Saint Paul, Minnesota, USA, 2012.

[12] I. Georgilas, G. Dagnino, P. Tarassoli, R. Atkins, and S. Dogramadzi, "Preliminary Analysis of Force-Torque Measurements for Robot-Assisted Fracture Surgery," in *EMBC 2015*, Milan, Italy, 2015.

[13] G. Dagnino, I. Georgilas, P. Tarassoli, R. Atkins, and S. Dogramadzi, "Design and Real-Time Control of a Robotic System for Fracture Manipulation," in *EMBC 2015*, Milan, Italy, 2015.

[14] G. Dagnino, I. Georgilas, P. Tarassoli, R. Atkins, and S. Dogramadzi, "Vision-based real-time position control of a semi-automated system for robot-assisted joint fracture surgery," *Int. J. Comput. Assist. Radiol. Surg.*, pp. 1–19, Oct. 2015.

[15] G. Dagnino, I. Georgilas, P. Tarassoli, R. Atkins, and S. Dogramadzi, "Intra-Operative 3D Imaging System for Robot-Assisted Fracture Manipulation," in *EMBC 2015*, Milan, Italy, 2015.

[16] G. Dagnino, L.S. Mattos, and D.G. Caldwell, "A vision-based system for fast and accurate laser scanning in robot-assisted phonomicrosurgery," *Int J Comput Assist Radiol Surg*, vol. 10, no. 2, pp. 217–229, 2015.

[17] C. Natale, "Quaternion-based representation of rigid bodies orientation," *PRISMA Technical Report*, vol. 97, no. 5, 1997.

[18] C. L. Phillips, T. Nagle, and A. Chakrabortty, *Digital Control System Analysis and Design*, 4th ed. Englewood Cliffs: Prentice Hall, 2015.

[19] C. Y. Chung WK, *PID trajectory tracking control for mechanical systems*. Berlin: Springer, 2008.

[20] J. H. Brown and S. A. DeLuca, "Growth plate injuries: Salter-Harris classification," *Am. Fam. Physician*, vol. 46, no. 4, pp. 1180–1184, Oct. 1992.